

Simulation of Triple Junction Motion with Arbitrary Surface Tensions

Nur Shofianah, Rhudaina Z. Mohammad, Karel Svadlenka

Abstract—We simulate triple junction motion that is given by the gradient flow of surface energy with arbitrary surface tensions of the individual interfaces. The foundation of the method is the diffusion-based BMO algorithm in vector-valued formulation. We modify the original vector-valued BMO method so that it can accommodate motions for any triple of surface tensions leading to the possibility of a nonsymmetric junction. The main idea of the modification is to adjust both the reference vectors and the coefficients in the underlying diffusion system. Moreover, we improve the method by using vector-valued projection triangle and also address the volume-preserving problem. Analysis and numerical results of this generalized vector-valued BMO algorithm are presented.

Index Terms—triple junction motion, mean curvature flow, surface tension, vector-valued thresholding

I. INTRODUCTION

THE problem of simulating the motion of interfaces with triple junction according to some curvature-dependent speed arises in many applications, e.g., grain growth [1], image processing [2], multiphase flow [3]. Equal surface tensions lead to symmetric triple junction, which is well-known as the symmetric Herring condition (interfaces meeting at 120°). On the other hand, arbitrary surface tensions lead to nonsymmetric triple junctions.

To treat such motions, several methods have been developed. Bronsard et. al [11] uses the reaction-diffusion equation

$$\mathbf{u}_t = \varepsilon \Delta \mathbf{u} - \frac{1}{\varepsilon} \nabla_{\mathbf{u}} W(\mathbf{u}), \quad (1)$$

to model triple junctions. Here, $\varepsilon > 0$ is a small parameter and W is a well potential, a non-negative function which has three minima for the three-phase case. This so-called phase-field method represents the phase boundary as an interfacial layer. In [11] the authors showed that the interfaces in the solution of (1) move with a velocity proportional to the curvature of the interface and in its sharp interface limit ($\varepsilon \rightarrow 0$), one obtains the Young's law at the junction. However, this method has difficulties in the numerical solution when $\varepsilon < \Delta x$, where Δx is the spacing grid. The only remedy is to take $\frac{\Delta x}{\varepsilon} \ll 1$, which is impractical numerically [4]. Moreover, it is also necessary to appropriately determine parameters of the well-potential function which

Manuscript received December 31, 2013; revised June 27, 2014. The work of the first author is supported by the Directorate General of Higher Education (DIKTI), Ministry of National Education, Indonesia and the second author by the Japanese Government (Monbukagakusho: MEXT) Scholarship Grant. This work was also supported by JSPS A3 Foresight Program "Computational Applied Mathematics 2014-2019".

Nur Shofianah and Rhudaina Z. Mohammad are with the Graduate School of Natural Science and Technology, Kanazawa University, 920-1192 Japan, e-mail: nur_shofianah@ub.ac.id, rhudaina@polaris.s.kanazawa-u.ac.jp

Karel Svadlenka is with Institute of Science and Engineering, Kanazawa University, 920-1192 Japan, and Institute of Mathematics, Academy of Sciences of the Czech Republic, Prague, Czech Republic, e-mail: kareru@staff.kanazawa-u.ac.jp

amounts to a complicated minimization problem. Garcke et al. [12] performed numerical simulations for a multiphase field model and showed that for suitably chosen parameters (which they determined based on numerical experiments), numerical results agree with the formal asymptotic expansion of [13] and yield the correct motion.

On the other hand, Zhao et al. [17] developed a numerical algorithm capturing the interfaces based on the level set method of Osher et al. [18]. This method is able to deal with topological singularities and nonsmooth data. Moreover, it can be extended to the multiphase setting by introducing as many level set functions as there are phases and imposing an additional constraint on the constrained flow problem so that the level sets do not overlap or create vacuums. However, such a constraint has an unwanted influence on the motion and the volume of phases is not sufficiently controlled by the method.

Merriman, Bence and Osher [4] introduced the BMO method, an implicit scheme for realizing interfacial motion by mean curvature for symmetric junctions, which alternately diffuses and sharpens characteristic function for each phase region. For two-phase case, it has been shown that the method converges to motion by mean curvature [5], [6], [7]. Ruuth [8] generalized the BMO method to nonsymmetric triple junctions by replacing the thresholding step with a new decision, i.e., by using a projection triangle. This generalized method also allows for normal velocity equal to a positive multiple of the curvature of the interface plus the difference in bulk energies for prescribed junction angles. Svadlenka et al. [3] reformulated the BMO algorithm in vector-valued formulation for multiphase motion. This vector-valued formulation is essential for implementing constraints and for dealing with more general motions. However, it is restricted to the symmetric case. Mohammad et al. [9], [10] improved the symmetric multiphase BMO algorithm of [3] by introducing a signed distance vector-valued function.

In this work, we consider three evolving curves meeting at a junction and having arbitrary surface tensions. We achieve the simulation of such a triple junction by generalizing the two main ingredients of the method in [3]: the reference vectors (corresponding to the positions of wells in the phase-field method) and the way of diffusing. Moreover, we improve the scheme by including a modification of the projection step in [8]. The developed method is applicable to constrained motions.

The outline of the paper is as follows: in Section II, we formulate the problem by deriving gradient flow of surface energy and computing the stable junction angles for given surface tensions. In Section III, we review the vector-valued BMO method of [3]. We discuss the junction stability in Section IV, where we derive the reference vectors of the BMO method. In Section V, we investigate the interface

velocity and find the suitable modification for the coefficients of underlying diffusion system. Section VI presents a correction by projection triangle. Numerical method and its implementation are explained in Section VII. Finally, Section VIII shows several numerical tests.

II. EQUATIONS OF TRIPLE JUNCTION

In this section, we write the total surface energy of the curves and compute its first variation to get the normal velocity for each interface and the condition that has to be satisfied at triple junction.

We consider three evolving curves $\gamma_i(s)$, $s \in [p_i, q_i]$, $i = 1, 2, 3$, which lie inside a fixed smooth region Ω of \mathbb{R}^2 , meet the outer boundary $\partial\Omega$ at a right angle and get together at a triple junction $x_T = \gamma_i(q_i)$, $i = 1, 2, 3$. Each curve has different surface tension σ_i .

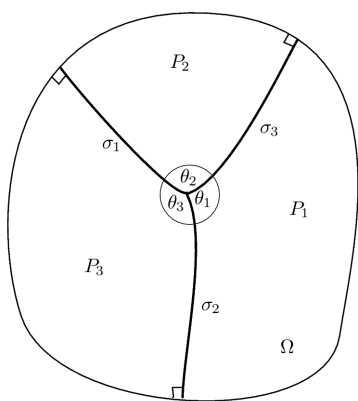


Fig. 1. Triple Junction

Then the surface energy of all curves is given by

$$L(\gamma) = \sum_{i=1}^3 \int_{\gamma_i} \sigma_i dl = \sum_{i=1}^3 \int_{p_i}^{q_i} \sigma_i |\gamma'_i(s)| ds.$$

The gradient flow of surface energy [19] can be found from its variation. Define the tangential vector t_i , curvature κ_i and outer normal n_i of curve γ_i by

$$t_i = \frac{\gamma'_i}{|\gamma'_i|}, \quad \kappa_i = -\frac{\gamma'_{ix}\gamma''_{iy} - \gamma'_{iy}\gamma''_{ix}}{|\gamma'_i|^3}, \quad n_i = \frac{1}{|\gamma'_i|}(\gamma'_{iy}, -\gamma'_{ix}).$$

Then for a smooth vector field φ vanishing near the boundary $\partial\Omega$,

$$\begin{aligned} \frac{d}{d\epsilon} L(\gamma + \epsilon\varphi(\gamma))|_{\epsilon=0} &= \sum_{i=1}^3 \int_{p_i}^{q_i} \sigma_i t_i \cdot \frac{d}{ds}(\varphi(\gamma_i)) ds \\ &= \sum_{i=1}^3 \left(- \int_{\gamma_i} (\sigma_i \kappa_i n_i) \cdot \varphi dl + \sigma_i t_i \cdot \varphi(x_T) \right). \end{aligned}$$

From this result, the motion by gradient flow satisfies

- 1) The normal velocity of interface

$$v_i = \sigma_i \kappa_i. \tag{2}$$

- 2) Condition at triple junction

$$\sum_{i=1}^3 \sigma_i t_i = 0. \tag{3}$$

The junction condition (3) is the balance of forces which is well-known to be equivalent to the Young's law

$$\frac{\sin \theta_1}{\sigma_1} = \frac{\sin \theta_2}{\sigma_2} = \frac{\sin \theta_3}{\sigma_3},$$

where $\theta_1, \theta_2, \theta_3$ are the angles at the junction (see Figure 1).

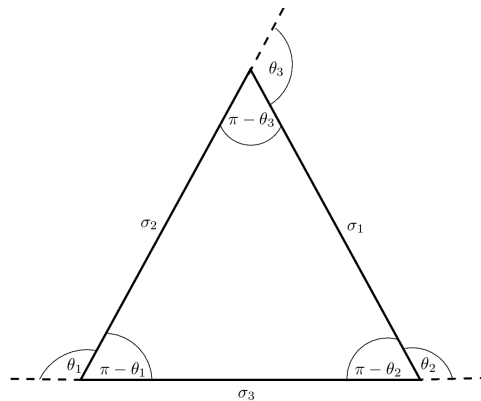


Fig. 2. Relating surface tensions to junction angles.

Noting the connection of the above formula to the triangle in Figure 2 and using the law of cosines, we obtain the junction angles as [14]:

$$\begin{aligned} \cos(\pi - \theta_1) &= \frac{\sigma_3^2 + \sigma_2^2 - \sigma_1^2}{2\sigma_2\sigma_3}, \\ \cos(\pi - \theta_2) &= \frac{\sigma_1^2 + \sigma_3^2 - \sigma_2^2}{2\sigma_1\sigma_3}, \end{aligned} \tag{4}$$

and $\theta_1 + \theta_2 + \theta_3 = 2\pi$.

Note that we can compute the stable angles with any given triple of surface tensions, as long as the triple satisfies the triangle inequality.

III. VECTOR-VALUED BMO

The basis of our method is the vector-valued BMO algorithm [3]:

- 1) Define reference vectors p_i of dimension two, each corresponding to a phase P_i for $i = 1, 2, 3$.
- 2) Given a partition P_i , $i = 1, 2, 3$, set $u_0(x) = p_i$ for $x \in P_i$.
- 3) Repeat

- Solve the vector-valued heat equation with initial condition u_0 :

$$\begin{aligned} u_t(t, x) &= \Delta u(t, x) \quad \text{for } (t, x) \in (0, \Delta t] \times \Omega, \\ \frac{\partial u}{\partial n}(t, x) &= 0 \quad \text{on } (0, \Delta t] \times \partial\Omega. \end{aligned}$$

- Update u_0 by identifying the reference vector which is closest to the solution $u(\Delta t, x)$:

$$u_0(x) = p_j,$$

$$\text{where } p_j \cdot u(\Delta t, x) = \max_{i=1,2,3} p_i \cdot u(\Delta t, x).$$

This redistribution of reference vectors determines the configuration of each phase after time Δt .

The paper [3] deals only with symmetric junctions and therefore, the above algorithm works with symmetric reference vectors and simple heat equation in the diffusion step, as is formally proved there. However, for arbitrary junction angles, this setting is not sufficient and has to be generalized. We will do so in the following two sections.

IV. JUNCTION STABILITY

We consider three straight lines meeting at the origin with the given stable angles as in Figure 3. The fact that this configuration is stable will yield a condition on the selection of reference vectors for the BMO algorithm.

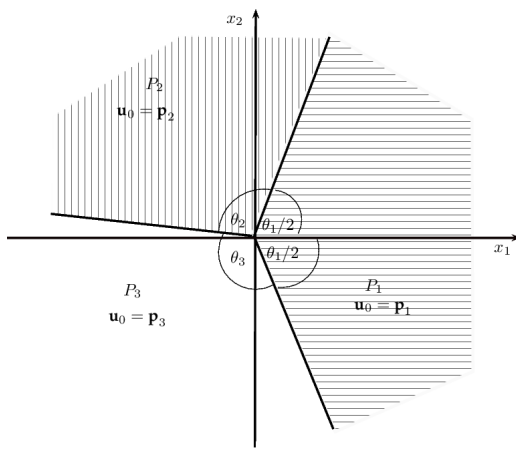


Fig. 3. Configuration of a stable junction.

The triple junction does not move if $\mathbf{u}(t, 0, 0) = \mathbf{0}$ for all $t > 0$, where \mathbf{u} is the solution of the heat equation. This means

$$\frac{1}{4\pi t} \sum_{i=1}^3 \mathbf{p}_i \int_{\mathbb{R}^2 \cap P_i} \exp\left(-\frac{|x|^2}{4t}\right) dx = \mathbf{0}.$$

Since by radial symmetry we can compute the integral of the wedge P_i as

$$\int_{P_i} e^{-|x|^2} dx = \frac{\theta_i}{2},$$

we get

$$\theta_1 \mathbf{p}_1 + \theta_2 \mathbf{p}_2 + \theta_3 \mathbf{p}_3 = \mathbf{0}. \tag{5}$$

The above relation is a one-dimension higher BMO analogue of Young's law (3) in the sense that the reference vectors \mathbf{p}_i are distributed in the whole phase regions P_i and, thus, the equilibrium condition is related to area integrals, which results in weights equal to junction angles.

The vector equation (5) and the condition obtained in the next section that the lengths of $\mathbf{p}_i, i = 1, 2, 3$, must be equal, form a systems of equations for the components of \mathbf{p}_i . Since the reference vectors are determined up to rotation and scaling, we can choose one reference vector arbitrarily, e.g., we set $\mathbf{p}_3 = (1, 0)$. This closes the system and its solution

can be written as

$$\begin{aligned} p_1^1 &= 1 - \frac{2\pi}{\theta_1\theta_3}(\pi - \theta_2), \\ p_1^2 &= \pm \frac{2}{\theta_1\theta_3} \sqrt{\pi(\pi - \theta_1)(\pi - \theta_2)(\pi - \theta_3)}, \\ p_2^1 &= 1 - \frac{2\pi}{\theta_2\theta_3}(\pi - \theta_1), \\ p_2^2 &= \mp \frac{2}{\theta_2\theta_3} \sqrt{\pi(\pi - \theta_1)(\pi - \theta_2)(\pi - \theta_3)}. \end{aligned} \tag{6}$$

The possible choices for the sign of the second component follow from the invariance of the reference vectors with respect to flipping.

V. INTERFACE VELOCITY

Here we study the modification of the original BMO algorithm yielding the correct interface velocities $v_i = \sigma_i \kappa_i$. The idea is to consider, instead of the heat equation, the general diffusion system

$$\begin{cases} u_t^1 + du_t^2 = a\Delta u^1 + b\Delta u^2, \\ du_t^1 + eu_t^2 = b\Delta u^1 + c\Delta u^2, \\ \begin{pmatrix} u^1 \\ u^2 \end{pmatrix} (t=0) = \begin{pmatrix} u_0^1 \\ u_0^2 \end{pmatrix}, \end{cases} \tag{7}$$

and determine its coefficients a, b, c, d, e , so that we obtain the desired interface velocities. We will show that this leads to a system of nonlinear equations for a, b, c, d, e . Moreover, we check that the change of the underlying diffusion system does not influence the arguments of the previous section on junction stability.

Note that we restrict our considerations to symmetric coefficient matrices. This is due to the fact that in order to incorporate phase-volume preservation, we use the variational structure of the system in an essential way (see Section VII.B).

The system (7) can be rewritten in the form

$$\tilde{\mathbf{u}}_t = A\Delta\tilde{\mathbf{u}},$$

where

$$\tilde{\mathbf{u}} = \begin{pmatrix} \tilde{u}^1 \\ \tilde{u}^2 \end{pmatrix} = \begin{pmatrix} 1 & d \\ d & e \end{pmatrix} \begin{pmatrix} u^1 \\ u^2 \end{pmatrix},$$

and

$$A = \frac{1}{e - d^2} \begin{pmatrix} ae - bd & b - ad \\ be - cd & c - bd \end{pmatrix}.$$

We assume that A is positive definite and diagonalize it in the following form

$$A = K\Lambda K^{-1} \quad \text{with} \quad \Lambda = \begin{pmatrix} \lambda_1 & 0 \\ 0 & \lambda_2 \end{pmatrix}.$$

The eigenvalues of A are given by

$$\lambda_{1,2} = \frac{ae + c - 2bd \pm r}{2(e - d^2)},$$

where $r = \sqrt{(ae - c)^2 + 4(ad - b)(cd - be)}$.

Hence, we get the matrix K consisting of eigenvectors as

$$K = \frac{1}{2r} \begin{pmatrix} ae - c + r & 2(ad - b) \\ 2(be - cd) & ae - c + r \end{pmatrix}.$$

The original problem is transformed into

$$\begin{cases} w_t^1 = \lambda_1 \Delta w^1, \\ w_t^2 = \lambda_2 \Delta w^2, \\ \begin{pmatrix} w^1 \\ w^2 \end{pmatrix} (t=0) = \begin{pmatrix} w_0^1 \\ w_0^2 \end{pmatrix} = M \begin{pmatrix} u_0^1 \\ u_0^2 \end{pmatrix}, \end{cases} \quad (8)$$

where $\begin{pmatrix} w^1 \\ w^2 \end{pmatrix} = M \begin{pmatrix} u^1 \\ u^2 \end{pmatrix}$, with $M = K^{-1} \begin{pmatrix} 1 & d \\ d & e \end{pmatrix}$.

The solution to the transformed problem (8) in the whole \mathbb{R}^2 is

$$w^i(t, x) = \frac{1}{4\pi\lambda_i t} \int_{\mathbb{R}^2} w_0^i(\xi) e^{-\frac{|x-\xi|^2}{4\lambda_i t}} d\xi, \quad i = 1, 2, \quad (9)$$

where

$$w_0^i|_{P_j} = ((M\mathbf{u}_0)|_{P_j})^i = (M\mathbf{p}_j)^i, \quad i = 1, 2, \quad j = 1, 2, 3.$$

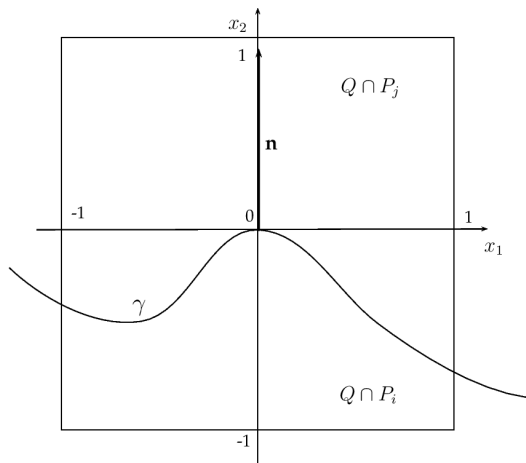


Fig. 4. Configuration of the interface.

Now, let us calculate the velocity of the interface for the above diffusion system. We consider a point on the interface $\gamma = \partial P_{ij}$ between phase P_i and P_j . We translate and rotate the coordinate system so that the chosen point lies in the origin and the outer normal to the point agrees with the positive x_2 -direction. We define $Q = [-1, 1] \times [-1, 1]$. Then the normal velocity v of the interface is found from the relation, expressing the condition on the interface position along the x_2 -axis after time t , i.e.,

$$\mathbf{u}(t, 0, vt) \cdot (\mathbf{p}_i - \mathbf{p}_j) = 0. \quad (10)$$

We can write the solution of the transformed problem (8) as

$$\mathbf{w}(t, 0, vt) = \begin{pmatrix} \frac{1}{4\pi\lambda_1 t} \int_{\mathbb{R}^2} w_0^1(\xi) e^{-\frac{|\xi-(0,vt)|^2}{4\lambda_1 t}} d\xi \\ \frac{1}{4\pi\lambda_2 t} \int_{\mathbb{R}^2} w_0^2(\xi) e^{-\frac{|\xi-(0,vt)|^2}{4\lambda_2 t}} d\xi \end{pmatrix}.$$

By the techniques in [5] and [15], we get

$$\frac{1}{4\pi\lambda_1 t} \int_{Q \cap P_i} e^{-\frac{|\xi-(0,vt)|^2}{4\lambda_1 t}} d\xi = \frac{1}{2} + \frac{\sqrt{t}}{2\sqrt{\pi\lambda_1}} (\lambda_1 \kappa - v) + O(t^{\frac{3}{2}}), \quad (11)$$

where κ is the curvature of ∂P_{ij} at the origin. Hence, we have for $l = 1, 2$, and some $C > 0$,

$$\begin{aligned} w^l(t, 0, vt) &= \frac{w_0^l|_{P_i}}{4\pi\lambda_l t} \int_{Q \cap P_i} e^{-\frac{|\xi-(0,vt)|^2}{4\lambda_l t}} d\xi \\ &\quad + \frac{w_0^l|_{P_j}}{4\pi\lambda_l t} \int_{Q \cap P_j} e^{-\frac{|\xi-(0,vt)|^2}{4\lambda_l t}} d\xi + O(e^{-\frac{C}{t}}) \\ &= w_0^l|_{P_i} \left(\frac{1}{2} + \frac{\sqrt{t}}{2\sqrt{\pi\lambda_l}} (\lambda_l \kappa - v) \right) \\ &\quad + w_0^l|_{P_j} \left(\frac{1}{4\pi\lambda_l t} \int_{\mathbb{R}^2} e^{-\frac{|\xi-(0,vt)|^2}{4\lambda_l t}} d\xi \right) \\ &\quad - w_0^l|_{P_j} \left(\frac{1}{2} + \frac{\sqrt{t}}{2\sqrt{\pi\lambda_l}} (\lambda_l \kappa - v) \right) + O(t^{\frac{3}{2}}) \\ &= w_0^l|_{P_i} \left(\frac{1}{2} + \frac{\sqrt{t}}{2\sqrt{\pi\lambda_l}} (\lambda_l \kappa - v) \right) \\ &\quad + w_0^l|_{P_j} \left(\frac{1}{2} - \frac{\sqrt{t}}{2\sqrt{\pi\lambda_l}} (\lambda_l \kappa - v) \right) + O(t^{\frac{3}{2}}) \\ &= \frac{w_0^l|_{P_i} + w_0^l|_{P_j}}{2} \\ &\quad + \frac{w_0^l|_{P_i} - w_0^l|_{P_j}}{2} \frac{\sqrt{t}}{\sqrt{\pi\lambda_l}} (\lambda_l \kappa - v) + O(t^{\frac{3}{2}}). \end{aligned}$$

We obtain from (10) the identity

$$M^{-1} \left[M \frac{\mathbf{p}_i + \mathbf{p}_j}{2} + \frac{\sqrt{t}}{\sqrt{\pi}} DM \frac{\mathbf{p}_i - \mathbf{p}_j}{2} \right] \cdot (\mathbf{p}_i - \mathbf{p}_j) = O(t^{\frac{3}{2}}),$$

where

$$D = \begin{pmatrix} \frac{1}{\sqrt{\lambda_1}} (\lambda_1 \kappa - v) & 0 \\ 0 & \frac{1}{\sqrt{\lambda_2}} (\lambda_2 \kappa - v) \end{pmatrix}.$$

Notice that if the first dot product on the left-hand side does not vanish, then the order in time of the equation does not match. This leads to the condition $(\mathbf{p}_i + \mathbf{p}_j) \cdot (\mathbf{p}_i - \mathbf{p}_j) = 0$, meaning that the lengths of reference vectors have to be equal (see Section IV). Then we obtain

$$(\mathbf{p}_i - \mathbf{p}_j)^T M^{-1} DM (\mathbf{p}_i - \mathbf{p}_j) = O(t),$$

which is, up to order $O(t)$, equivalent to

$$\mu_1 \left(\sqrt{\lambda_1} \kappa - \frac{1}{\sqrt{\lambda_1}} v \right) + \mu_2 \left(\sqrt{\lambda_2} \kappa - \frac{1}{\sqrt{\lambda_2}} v \right) = 0,$$

where

$$\begin{aligned} \mu_1 &= m_{11}m_{22}(p_{ij}^1)^2 - m_{12}m_{21}(p_{ij}^2)^2 \\ &\quad + (m_{12}m_{22} - m_{11}m_{21})p_{ij}^1 p_{ij}^2, \\ \mu_2 &= -m_{12}m_{21}(p_{ij}^1)^2 + m_{11}m_{22}(p_{ij}^2)^2 \\ &\quad - (m_{12}m_{22} - m_{11}m_{21})p_{ij}^1 p_{ij}^2, \end{aligned}$$

with $\mathbf{p}_{ij} = \mathbf{p}_i - \mathbf{p}_j$ and $m_{11}, m_{12}, m_{21}, m_{22}$ denote the entries of the matrix M . Finally, we get the velocity of interface γ_k ($k \neq i, j$) in the form

$$v_k = \frac{\mu_1 \sqrt{\lambda_1} + \mu_2 \sqrt{\lambda_2}}{\mu_2 \sqrt{\lambda_1} + \mu_1 \sqrt{\lambda_2}} \sqrt{\lambda_1 \lambda_2} \kappa_k.$$

Since there are only three types of interfaces, it is expected that we need only three parameters in order to design the

velocities. Hence, it is reasonable to try to set $d = 0, e = 1$, so that our diffusion system becomes

$$\mathbf{u}_t = A\Delta\mathbf{u}, \tag{12}$$

with $A = \begin{pmatrix} a & b \\ b & c \end{pmatrix}$. We could have done so from the beginning of this section but, as we will see below, the resulting nonlinear system for a, b, c is hard to analyze theoretically, which led us to keep the parameters d and e as a last resort in case the three-parameter system cannot be solved. In this case, we get the interface velocities

$$v_k = \frac{\mu_1(a + c + r) + 2\mu_2\sqrt{ac - b^2}}{\mu_2(a + c + r) + 2\mu_1\sqrt{ac - b^2}} \sqrt{ac - b^2} \kappa_k, \tag{13}$$

where $r = \sqrt{(a - c)^2 + 4b^2}$ and

$$\begin{aligned} \mu_1 &= [(a - c + r)(p_i^1 - p_j^1) + 2b(p_i^2 - p_j^2)]^2, \\ \mu_2 &= [2b(p_i^1 - p_j^1) - (a - c + r)(p_i^2 - p_j^2)]^2. \end{aligned}$$

From (13) and (2), we have a nonlinear system consisting of three equations for the coefficients a, b and c , which is solved numerically. First, we simplify it by setting

$$\begin{aligned} x &= \frac{\alpha + \sqrt{\beta^2 + 1}}{\sqrt{\alpha^2 - \beta^2 - 1}}, \\ y &= \beta + \sqrt{\beta^2 + 1}, \\ z &= b\sqrt{\alpha^2 - \beta^2 - 1}, \end{aligned}$$

where $\alpha = (a + c)/(2b)$ and $\beta = (a - c)/(2b)$. Then the above system in terms of x, y, z becomes

$$\frac{(p_{ij}^1 y + p_{ij}^2)^2 x + (p_{ij}^1 - p_{ij}^2 y)^2}{(p_{ij}^1 - p_{ij}^2 y)^2 x + (p_{ij}^1 y + p_{ij}^2)^2} z = \sigma_k$$

for $(i, j, k) = (2, 3, 1), (1, 3, 2), (1, 2, 3)$. We take any two equations from this system and solve for x, z analytically, which is possible, since the corresponding equation is quadratic. Due to this fact we get two different solutions for x, z . For each such pair of x, z we use a numerical method (such as Newton's method) to find the root y of the remaining equation. There may exist several roots for y . For each such combination of x, y, z we recover α, β and b by

$$\alpha = \frac{(x^2 + 1)(y^2 + 1)}{2(x^2 - 1)y}, \quad \beta = \frac{y^2 - 1}{2y}, \quad b = \pm \frac{x(y^2 + 1)}{(x^2 - 1)y}.$$

The coefficients a and c are then obtained easily. The number of cases doubles because of two possible signs for b . All triples (a, b, c) obtained in the described way are then checked if they solve the system and the appropriate triple is selected.

Since the nonlinear system is very complicated, we were not able to prove the unique existence of solution using analytical methods such as fixed point theory. However, in using the above method we can always find a solution, except when $b = 0$, which occurs when two of the surface tensions are equal. In that case, the system simplifies in such a way that it can be solved fully analytically.

Remark. For the initial condition in Figure 3, at the triple junction we have

$$\begin{aligned} w^i(t, 0) &= \frac{1}{4\pi\lambda_i t} \left(\int_{P_1} + \int_{P_2} + \int_{P_3} \right) w_0^i(\xi) e^{-\frac{|\xi|^2}{4\lambda_i t}} d\xi \\ &= \frac{1}{\pi} \left(\frac{\theta_1}{2} w_0^i|_{P_1} + \frac{\theta_2}{2} w_0^i|_{P_2} + \frac{\theta_3}{2} w_0^i|_{P_3} \right). \end{aligned}$$

Therefore,

$$\mathbf{w}(t, 0) = \frac{1}{2\pi} M (\theta_1 \mathbf{p}_1 + \theta_2 \mathbf{p}_2 + \theta_3 \mathbf{p}_3).$$

For junction stability, we require $\mathbf{u}(t, 0) = M^{-1} \mathbf{w}(t, 0) = \mathbf{0}$. This condition is equivalent to

$$\theta_1 \mathbf{p}_1 + \theta_2 \mathbf{p}_2 + \theta_3 \mathbf{p}_3 = \mathbf{0},$$

which is in agreement with (5).

This result shows that no matter how we change the diffusion equation, the stability condition (5) will not be affected. Hence, the selection of reference vectors can be done independently of the diffusion equation.

VI. CORRECTION BY PROJECTION TRIANGLE

In the previous sections, we have derived an extension of the vector-valued BMO algorithm to include the case of nonsymmetric junctions and general interface velocities. We have shown that, for a suitably selected diffusion system, if an interface point is sufficiently far from the junction, the interface velocity at that point will satisfy the desired formula $v_i = \sigma_i \kappa_i$, and that, for a suitably selected reference vectors, the junction will be stationary for the initial configuration of three straight lines meeting at the junction with stable contact angles.

However, the above analysis does not address the close vicinity of the triple junction. In fact, by formal calculations it can be made clear (see Appendix A) that the correct interface velocity is obtained only with an exponentially decreasing error with respect to the distance of the considered interface point to the junction. Indeed, numerical tests proved that the stable configuration consisting of three straight lines slightly curves in the neighborhood of the junction. This fact produces errors in the angles of the moving junction.

Therefore, we include a correction step based on the notion of a projection triangle given by Ruuth [8]. The idea is to first investigate how the stable configuration of three straight lines deforms, and use this information to project the phase regions back into the correct position in each step of the BMO algorithm. For details of the construction of the projection triangle we refer to [8].

The original method in [8] uses the scalar setting, i.e., it diffuses separately characteristic functions for each of the three phase regions of the stable configuration (Figure 3) which yields three values of diffused function at every point in the domain. These three values are positive and sum up to one, thus, taken as points in \mathbb{R}^3 , lie inside a triangle on a hyperplane of \mathbb{R}^3 . The straight lines of the stable configuration are mapped on the triangle as dividing curves. In order to relate our vector-valued formulation to the construction in [8], for $(i, j, k) \in \{(1, 2, 3), (2, 3, 1), (3, 2, 1)\}$ we introduce the functions

$$f_i(t, x) = \frac{\mathbf{u}(t, x) \cdot (\mathbf{p}_j + \mathbf{p}_k) - 1 - \mathbf{p}_j \cdot \mathbf{p}_k}{(\mathbf{p}_i - \mathbf{p}_j) \cdot (\mathbf{p}_j + \mathbf{p}_k)}, \tag{14}$$

Note that (14) is a generalization of the function $w_i(t, x)$ in [3], Section 2.2.2, for general reference vectors (6). Since $\mathbf{u}(0, x) = \mathbf{p}_i$ for $x \in P_i$, one can easily check that

$$f_i(0, x) = \chi_i(x), \quad i = 1, 2, 3,$$

where χ_i is the characteristic function of phase region P_i .

However, the advantage of our vector-valued approach is that we do not have to perform separate diffusions and subsequently identify the hyperplane $x_1 + x_2 + x_3 = 1$. It is sufficient to diffuse the vector-valued initial condition as in Figure 3 and record the images of the straight lines. In this way, we obtain a projection triangle that can be used directly for the function \mathbf{u} in the BMO algorithm.

We summarize the construction of the projection triangle in the generalized vector-valued formulation. Given an angle configuration $\theta_1, \theta_2, \theta_3$, we perform the following steps:

- 1) Define the lines (in polar coordinates)

$$\ell_{12} = \left\{ \left(r, \frac{1}{2}\theta_1 \right) : r > 0 \right\},$$

$$\ell_{13} = \left\{ \left(r, -\frac{1}{2}\theta_1 \right) : r > 0 \right\},$$

$$\ell_{23} = \left\{ \left(r, \frac{1}{2}\theta_1 + \theta_2 \right) : r > 0 \right\},$$

and regions P_1, P_2, P_3 , as in Figure 3.

- 2) Set $\mathbf{u}_0(x) = \mathbf{p}_i$ for $x \in P_i$.
- 3) Apply the diffusion (7) to the initial condition \mathbf{u}_0 for a time $\tau \leq \Delta t$, where Δt is the BMO time step.
- 4) Map the values of the solution of step 3 along each line ℓ_{ij} onto the projection triangle to form the dividing lines $\tilde{\ell}_{ij}$: $\tilde{\ell}_{ij} = \{ \mathbf{u}(\tau, x) : x \in \ell_{ij} \}$.

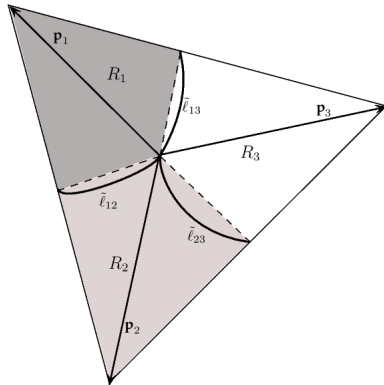


Fig. 5. Projection triangle \mathcal{T} in vector-valued setting.

Notice that the values of the diffused function \mathbf{u} fall inside the triangle \mathcal{T} formed by the vectors $\mathbf{p}_1, \mathbf{p}_2, \mathbf{p}_3$ (Figure 5). Moreover, because of (5), the dividing lines $\tilde{\ell}_{12}, \tilde{\ell}_{13}, \tilde{\ell}_{23}$ will always meet at the origin which corresponds to the circumcenter of \mathcal{T} , and they approach the midpoints of edges of \mathcal{T} on their other ends. This is in contrast to the projection triangles in [8], where the position of the junction shifts and the shape of dividing lines is distorted, especially for junction angles strongly deviating from the Herring symmetric case. This fact helps significantly to make the numerical computations stable, especially for the volume-preserving problem.

Figure 6 shows the resulting projection triangles for the $150^\circ - 90^\circ - 120^\circ$ junction and the $135^\circ - 90^\circ - 135^\circ$ junction. Since these two cases will be used in numerical tests, we list the corresponding parameters in Table I. As it sometimes happens in the numerical computations that the values of the function \mathbf{u} fall out of the projection triangle, we extend the dividing curves by straight lines connecting the junction to the midpoints of the edges.

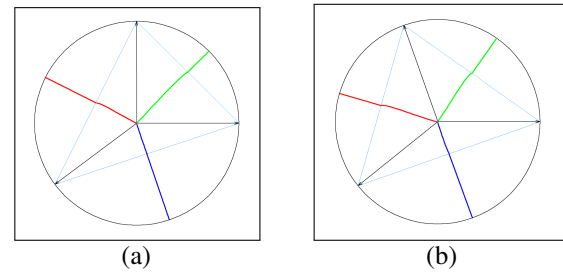


Fig. 6. Projection triangle for (a) $150^\circ - 90^\circ - 120^\circ$ and (b) $135^\circ - 90^\circ - 135^\circ$ triple junctions.

TABLE I
NUMERICAL PARAMETERS FOR CASE 1 AND CASE 2

parameters		case 1	case 2
surface tensions	σ_1	$\frac{1}{2}$	$\frac{\sqrt{2}}{2}$
	σ_2	1	1
	σ_3	$\frac{\sqrt{3}}{2}$	$\frac{\sqrt{2}}{2}$
angles	θ_1	150°	135°
	θ_2	90°	90°
	θ_3	120°	135°
coefficients	a	0.881	0.954
	b	0.262	0.127
	c	0.656	0.639
reference vectors	\mathbf{p}_1	(-0.8,-0.6)	(-0.777,-0.628)
	\mathbf{p}_2	(0,1)	(-0.333,-0.943)
	\mathbf{p}_3	(1,0)	(1,0)

Remark. There is a close relation between the BMO algorithm and a splitting method for the phase-field equation (1), which repeats the following steps:

- 1) Diffuse for a time Δt

$$\mathbf{u}_t = \varepsilon \Delta \mathbf{u},$$

with initial condition $\mathbf{u}(0, x) = \mathbf{u}_0$.

- 2) Solve

$$\mathbf{u}_t = -\frac{1}{\varepsilon} W'(\mathbf{u}), \quad (15)$$

with initial condition $\mathbf{u}(\Delta t, x)$.

One can see that (15) corresponds to the thresholding step in BMO in the sense that the solution asymptotically separates into three regions with values equal to the minima of W . The dividing lines between these regions are the separatrices for the well potential W . The well potential can be chosen as in [12] but, as mentioned in the Introduction, it is not easy to calibrate its parameters since they are not given by an explicit formula.

VII. THE ALGORITHM

In this section, we summarize the above deliberations into a generalized vector-valued BMO scheme. First we present the basic version of the BMO algorithm and then comment on the method of incorporating the volume constraint.

A. Generalized vector-valued BMO algorithm

The generalized vector-valued BMO for three-phases motion is as follows:

- 1) For given surface tensions, calculate junction angles θ_i by (4).
- 2) Define reference vectors \mathbf{p}_i according to formula (6).

- 3) Find the solution a, b, c of (13) and set $A = \begin{pmatrix} a & b \\ b & c \end{pmatrix}$.
- 4) Construct projection triangle according to the algorithm in Section VI.
- 5) For a given three phase initial configuration P_1, P_2, P_3 , set

$$\mathbf{u}_0(x) = \mathbf{p}_i, \quad x \in P_i.$$

- 6) Repeat until desired time
 - Solve the diffusion system

$$\mathbf{u}_t = A\Delta\mathbf{u} \quad \text{for } (t, x) \in (0, \Delta t] \times \Omega, \quad (16)$$

$$\frac{\partial \mathbf{u}}{\partial \mathbf{n}} = 0 \quad \text{on } (0, \Delta t] \times \Omega,$$

$$\mathbf{u}(0, x) = \mathbf{u}_0(x) \quad \text{in } \Omega.$$

- Threshold according to the projection triangle defined in step 4, i.e.,

$$\mathbf{u}_0(x) = \mathbf{p}_i \quad \text{if } \mathbf{u}(x) \in R_i, \quad i = 1, 2, 3,$$

where R_i are the regions in Figure 5.

The modified diffusion system is solved by using vector-type discrete Morse flow (DMF) [16], i.e., at each step we solve (16) by discretizing time $\Delta t = h \times N$ and successively minimizing the following functionals for $n = 1, \dots, N$ over $H^1(\Omega; R^2)$:

$$J_n(\mathbf{u}) = \int_{\Omega} \left(\frac{a}{2} |\nabla u^1|^2 + b \nabla u^1 \cdot \nabla u^2 + \frac{c}{2} |\nabla u^2|^2 \right) dx + \int_{\Omega} \left(\frac{|\mathbf{u} - \mathbf{u}_{n-1}|^2}{2h} \right) dx. \quad (17)$$

We approximate the functional (17) by using piecewise linear finite elements. The minimizers are found by steepest descent method.

B. BMO algorithm with volume-constraint

The minimization formulation of the vector-valued algorithm allows the inclusion of volume constraints via penalization. In particular, instead of the functional J_n in step 6, we minimize

$$F_n(\mathbf{u}) = J_n(\mathbf{u}) + \frac{1}{\epsilon} \sum_{i=1}^3 |V_i - \text{meas}(P_i^{\mathbf{u}})|^2.$$

Here $\epsilon > 0$ is a small penalty parameter, V_i is the prescribed volume of region P_i and the volumes corresponding to \mathbf{u} are obtained from the sets

$$P_i^{\mathbf{u}} = \{x \in \Omega; \mathbf{u}(x) \in R_i\}.$$

This means that we have to employ the projection triangle each time we evaluate the functional F_n .

VIII. NUMERICAL RESULTS

We now present some numerical tests and examples of our method. All numerical experiments in this section are conducted on a $[0, 1] \times [0, 1]$ domain with time step $\Delta t = 0.005$ and DMF partition $N = 30$. Moreover, the phase interior angles at the triple junction are measured using the tangents to the quadratic interpolation of the piecewise linear interface in the neighborhood of the junction.

We begin by investigating the stability of the triple junction in terms of the angle measure and location of the junction.

Next, we look at the behavior of the triple junction motion for two cases (with and without axial symmetry). Finally, we present an example which incorporates the volume constraint and check the stability of the junction and preservation of the phase volumes of its stationary solution.

A. Junction Stability Test

Consider an initial condition where phase P_2 consists of two disjoint square regions on opposite corners of the domain; while the remaining regions above and below the line $y = x$ are taken as phase P_1 and P_3 , respectively (refer to Figure 7a). In this setting, the interface network remains stationary for a $135^\circ-90^\circ-135^\circ$ junction angle configuration. We then, run our method under the case 2 setting (see Table I) and check the stability of the triple junction when the maximum dot product (without projection triangle) or projection triangle is used for phase detection. Here, the domain is triangulated into 12,800 elements ($\Delta x = 0.0125$).

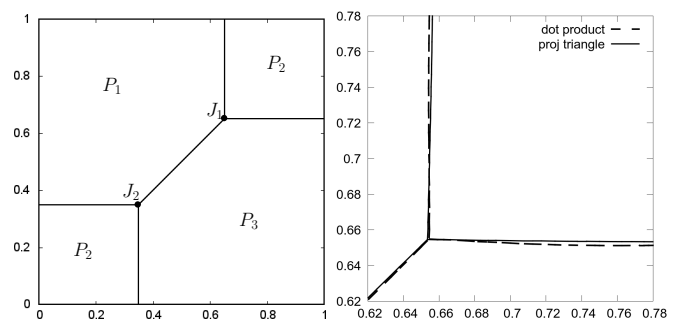


Fig. 7. (a) Initial condition. (b) The stationary interface network around junction J_1 after time $100\Delta t$ using dot product and projection triangle for phase detection.

The relative error of the stationary junction angle measures are summarized in Table II. We see that when the maximum dot product is used to locate the interface, the stationary interior angle in phase P_2 is of measure $90^\circ \pm 5.11$, while the other two junction angles are approximately $135^\circ \pm 4.10$; thereby, yielding a relative error of at most 5.68%. On the other hand, utilizing the projection triangle in the phase detection scheme reduces the relative error to at most 0.88% with stationary junction angles of measure $90^\circ \pm 0.78$ and $135^\circ \pm 1.19$.

TABLE II
RELATIVE ERROR IN JUNCTION ANGLE MEASURES

phase	maximum dot product		projection triangle	
	junction J_1	junction J_2	junction J_1	junction J_2
P_1	-0.0083	-0.0081	0.0088	0.0077
P_2	-0.0290	-0.0296	-0.0062	-0.0019
P_3	0.0561	0.0568	-0.0039	-0.0087

In addition, both phase detection scheme shifted the junction to a distance of at most 0.0065 for the dot product scheme and at most 0.0057 for the projection triangle. This can be accounted for by the approximation error in the construction of the projection triangle. Hence, our method stably preserves the angle conditions, in this case $135^\circ-90^\circ-135^\circ$. This also confirms that using the projection triangle in the phase detection scheme correctly detects the interface near the junction, as opposed to using the maximum dot product.

B. Triple Junction Motion

In this section, we start with an initial condition where a T-shaped interface is rotated 90° counterclockwise where the T-junction is at point (0.25, 0.5). We take phase P_2 as the region to the left of line $x = 0.25$, and the remaining top and bottom regions as phases P_1 and P_3 , respectively. We triangulate the domain into 20,000 elements with $\Delta x = 0.01$, and evolve the interface via our method using the projection triangle to determine the different phase regions at each time step. We then investigate the evolution of the triple junction in both cases.

1) *Junction without Axial Symmetry:* (Case 1 in Table I) Under the first case setup, we plot the evolution of the initial T-junction and its underlying interface network at different times in Figure 8.

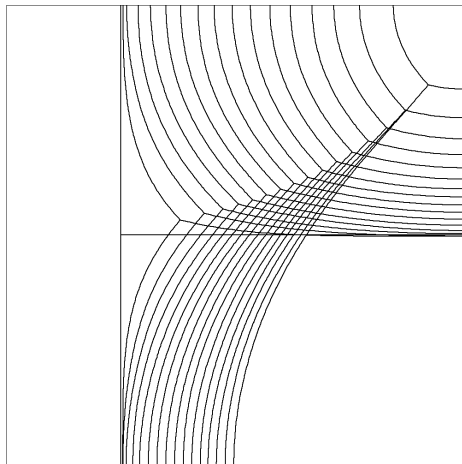


Fig. 8. Evolution of the triple junction for case 1.

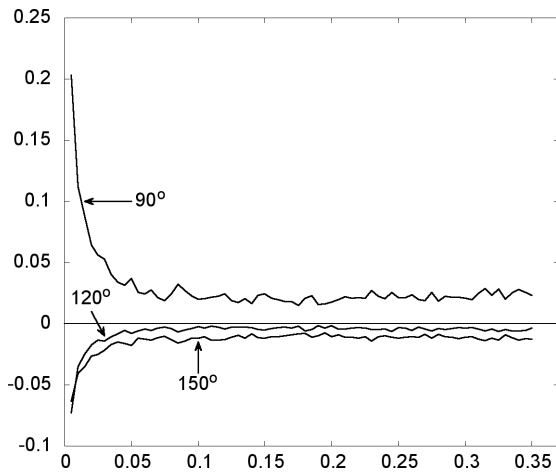


Fig. 9. Relative error of the junction angles at each time step.

Notice that for the first 10 time steps, the junction angles rapidly adjusts to approximate the 150°–90°–120° angle conditions. Thereafter, the triple junction maintains phase interior angles of measure within 2.5% relative error (refer to Figure 9). Note that this approximation error in the stationary junction angles can be made smaller by increasing the precision in the construction of the projection triangle.

2) *Axially Symmetric Junction:* (Case 2 in Table I) We now look at the behavior of the junction motion when subjected to the second case. Note that since the surface

tensions on the 1–2 and 2–3 interfaces are equal, that is, $\sigma_1 = \sigma_3 = \frac{1}{\sqrt{2}}$, we expect these interfaces to symmetrically evolve with respect to the horizontal line $y = 0.5$. This is in agreement with our numerical simulation shown in Figure 10.

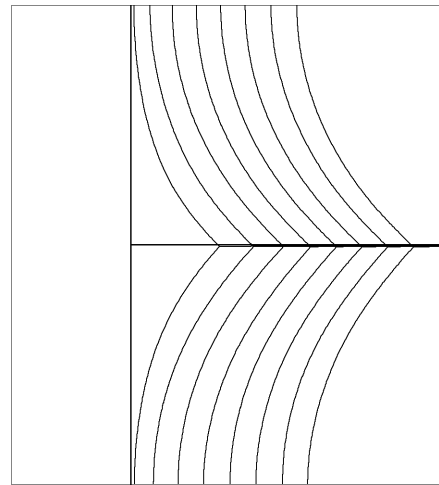


Fig. 10. Evolution of the triple junction for case 2.

In the first 10 time steps, the triple junction rapidly approaches the 135°–90°–135° angle conditions. After which, the interface gradually starts to move horizontally to the right. The transport velocity s of our numerical interface solution approaches $\frac{\pi}{2\sqrt{2}}$, which is the exact velocity of the constantly transported solution of the sharp interface problem, as shown in Figure 11.

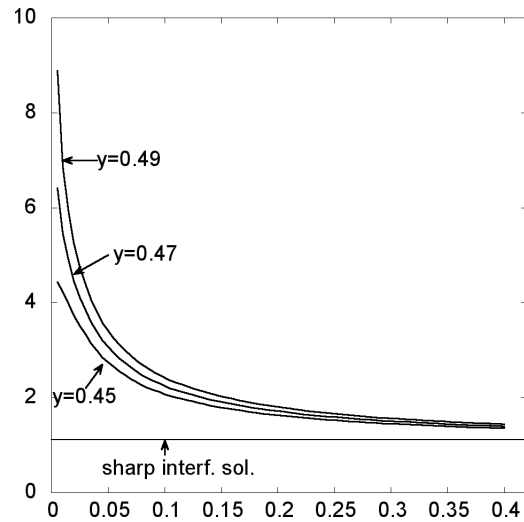


Fig. 11. Transport velocities of the numerical interface solution at $y = 0.45, 0.47, 0.49$ vs the constantly transported solution (sharp interf. sol.).

Moreover, we note that the shape of such a constantly transported profile in the axially symmetric case is determined by:

$$v(y) = -\frac{\sigma_1}{s} \log(\cos(\frac{s}{\sigma_1}y)) + c,$$

where the constant c of horizontal shift may be chosen appropriately [12]. Comparing this with the numerical interface solution obtained via our method, we see that it is in a good agreement with the exact shape of the profile (Figure 12).

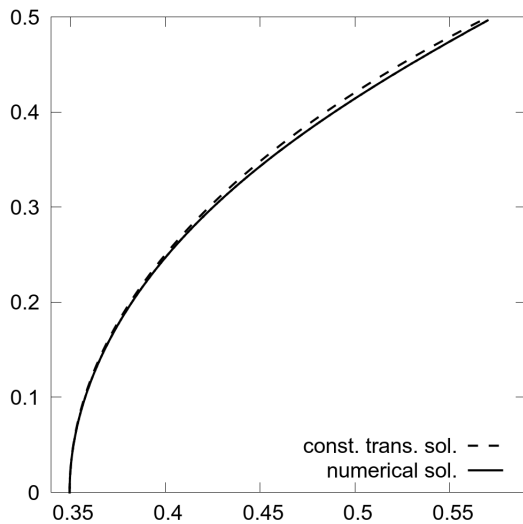


Fig. 12. The shape of the numerical interface at time $t = 30\Delta t$ vs the constantly transported solution.

C. Volume-preserving $150^\circ-90^\circ-120^\circ$ Double Bubble

Consider a three-phase volume-preserving case where two phases are identical squares with one common side of length 0.28. We take the outside region as phase P_1 , and the left and right square regions as phase P_2 and P_3 , respectively (refer Figure 13).

We evolve this configuration via our method under case 1 setting in Table I. Moreover, we wish to preserve the volume of each phase region employing a penalization technique with parameter $\epsilon = 10^{-6}$. Here, the domain is triangulated into 12,800 elements with $\Delta x = 0.0125$. To locate the interface, we use a projection scheme determined by the maximum dot product. The numerical stationary interface solution is shown in Figure 13.

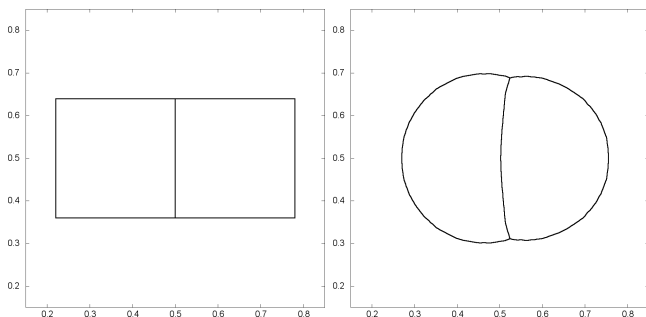


Fig. 13. (a) Initial Condition. (b) The stationary numerical solution in case 1.

To check the stability of the triple junction, we measure the junction angles at each time step and calculate the corresponding errors. We observe that the interior phase angles at the top and bottom triple junctions behave in the same manner, hence, we only plot the relative error in the measure of the top junction angle in Figure 14.

It is evident from the error plot that the triple junction first rapidly approximates the angle conditions, which is consistent with the previous results. Thereafter, the numerical solution gradually reaches a stationary state whose junction angles are of measure $150^\circ \pm 1.50$, $120^\circ \pm 2.43$, and $90^\circ \pm 1.36$ yielding a relative error of at most 2%. This is consistent with the result in our stability test. Hence, one can achieve

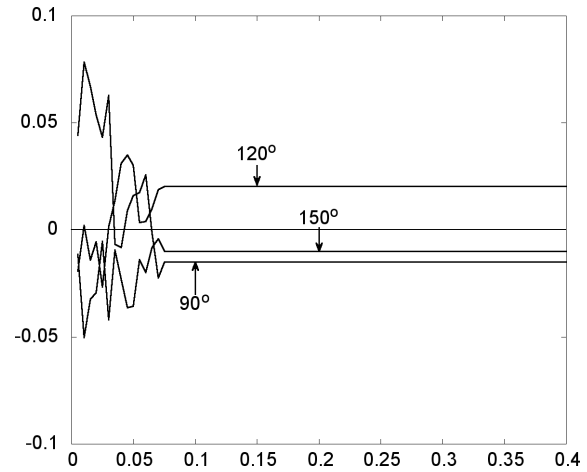


Fig. 14. Relative error of the top junction angles at each time step.

a more precise result using the projection triangle to locate the interface.

TABLE III
PHASE VOLUMES UNDER PENALTY PARAMETER $\epsilon = 10^{-6}$.

phase	prescribed vol	stationary state vol	absolute error
P_1	0.8432	0.84321	1.0×10^{-5}
P_2	0.0784	0.07840	3.0×10^{-6}
P_3	0.0784	0.07839	8.0×10^{-6}

Moreover, it is clear from Table III that the phase volumes are preserved. Hence, the stationary numerical solution obtain using our method fairly approximates the volume-preserving solution of case 1.

IX. CONCLUSION

We have developed a method for numerical realization of triple junction motion with arbitrary surface tensions. Our method is based on the vector-valued BMO algorithm, which has been generalized and augmented by a correction step using projection triangle. Several numerical tests, including the volume-constrained motion, were performed.

APPENDIX A
FORMAL ANALYSIS OF NONSYMMETRIC TRIPLE JUNCTION

We look at the formula for the solution of the system (7) with initial condition as in Figure 3 in more detail. From this, we will see that the interfaces close to the triple junction will not remain straight but will curve slightly.

Recalling the solution of the transformed problem (9), the solution of the original system is given by

$$\mathbf{u}(t, x) = M^{-1}w = M^{-1} \begin{pmatrix} w^1 \\ w^2 \end{pmatrix}, \quad (18)$$

where w^1, w^2 are obtained from the formula

$$w^i(t, x) = \left(\sum_{j=1}^3 (M\mathbf{p}_j)^i \int_{P_j} \right) \frac{1}{4\pi\lambda_i t} e^{-\frac{|x-\xi|^2}{4\lambda_i t}} d\xi, \quad i = 1, 2.$$

Set

$$\text{erfc}(s) = 1 - \text{erf}(s) = \frac{2}{\sqrt{\pi}} \int_s^\infty e^{-\sigma^2} d\sigma,$$

and

$$\alpha(\vartheta) = x_1 \cos \vartheta + x_2 \sin \vartheta,$$

$$\beta(\vartheta) = x_1 \sin \vartheta - x_2 \cos \vartheta.$$

To see the specific form of the respective terms, we compute the integral

$$\int_{P_1} e^{-\frac{|x-\xi|^2}{4\lambda t}} d\xi$$

$$= \int_0^\infty \int_{-\frac{\theta_1}{2}}^{\frac{\theta_1}{2}} e^{-\frac{(r-\alpha(\vartheta))^2 + \beta(\vartheta)^2}{4\lambda t}} r d\vartheta dr$$

$$= \int_{-\frac{\theta_1}{2}}^{\frac{\theta_1}{2}} e^{-\frac{\beta(\vartheta)^2}{4\lambda t}} \int_{-\frac{\alpha(\vartheta)}{\sqrt{4\lambda t}}}^\infty (\sqrt{4\lambda t}z + \alpha(\vartheta)) \sqrt{4\lambda t} e^{-z^2} dz d\vartheta$$

$$= \sqrt{\pi\lambda t} \int_{-\frac{\theta_1}{2}}^{\frac{\theta_1}{2}} \alpha(\vartheta) e^{-\frac{\beta(\vartheta)^2}{4\lambda t}} \operatorname{erfc}\left(-\frac{\alpha(\vartheta)}{\sqrt{4\lambda t}}\right) d\vartheta$$

$$+ 2\lambda t \int_{-\frac{\theta_1}{2}}^{\frac{\theta_1}{2}} e^{-\frac{\beta(\vartheta)^2 + \alpha(\vartheta)^2}{4\lambda t}} d\vartheta.$$

Rearranging the terms, we get

$$\int_{P_1} e^{-\frac{|x-\xi|^2}{4\lambda t}} d\xi$$

$$= 2\lambda t \sqrt{\pi} \int_{\frac{\beta(-\frac{\theta_1}{2})}{\sqrt{4\lambda t}}}^{\frac{\beta(\frac{\theta_1}{2})}{\sqrt{4\lambda t}}} e^{-z^2} \operatorname{erfc}\left(\pm \sqrt{\frac{|x|^2}{4\lambda t} - z^2}\right) dz$$

$$+ 2\lambda t \theta_1 e^{-\frac{|x|^2}{4\lambda t}}.$$

Expressing the point x in polar coordinates as $x = (s \cos \varphi, s \sin \varphi)$, we get

$$\frac{1}{2\lambda t} \int_{P_1} e^{-\frac{|x-\xi|^2}{4\lambda t}} d\xi$$

$$= \sqrt{\pi} \int_{\frac{s \sin(\frac{\theta_1}{2} - \varphi)}{\sqrt{4\lambda t}}}^{\frac{s \sin(\frac{\theta_1}{2} + \varphi)}{\sqrt{4\lambda t}}} e^{-z^2} \operatorname{erfc}\left(\pm \sqrt{\frac{s^2}{4\lambda t} - z^2}\right) dz$$

$$+ \theta_1 e^{-\frac{s^2}{4\lambda t}}, \tag{19}$$

and similarly for the integrals over the regions P_2 and P_3 . From (19) we can conclude that:

- 1) If $\frac{s}{\sqrt{t}}$ is close to zero, (19) approaches θ_1 since the first term is negligible. Hence, from (18) we get the value of the solution

$$\mathbf{u}(t, x) \approx \frac{\theta_1}{2\pi} \mathbf{p}_1 + \frac{\theta_2}{2\pi} \mathbf{p}_2 + \frac{\theta_3}{2\pi} \mathbf{p}_3,$$

which is in agreement with (5).

- 2) If the point x is away from the triple junction and close to some of the interfaces, for instance the interface between phases P_1 and P_2 , then the second term is exponentially small. Moreover, $\varphi \approx \frac{\theta_1}{2}$, and so the first integral will be close to π . Similarly, the integral over the region P_2 will be close to π and the integral over P_3 will be close to zero. Therefore, the solution (18) at this point x will be

$$\mathbf{u}(t, x) \approx \frac{1}{2}(\mathbf{p}_1 + \mathbf{p}_2),$$

which means that the interface will remain stationary as a straight line.

- 3) If the point x is in other position than the two cases mentioned above, the values of the above integrals will depend not only on x and t but also on the values of λ_1, λ_2 . As a consequence, the solution \mathbf{u} will depend also on the coefficients a, b, c , and the corresponding interfaces may curve.

REFERENCES

- [1] M. Elsey, S. Esodoglu, P. Smereka, "Diffusion generated motion for grain growth in two and three dimensions," in *J. Comp. Physics*, vol. 228, pp. 8015-8033, 2010.
- [2] F. Catte, P. L. Lions, J. M. Morel, "Image selective smoothing and edge detection by nonlinear diffusion," in *SIAM J. Num. Anal.*, vol. 29, pp. 182-183, 1992.
- [3] K. Svadlenka, E. Ginder, S. Omata, "A variational method for multiphase volume-preserving interface motions," in *Journal of Computational and Applied Mathematics*, vol. 257, pp. 157-179, 2014.
- [4] B. Merriman, J. Bence, S. Osher, "Motion of multiple junctions: a level set approach," in *J. Comp. Physics*, vol. 112, pp. 334-363, 1994.
- [5] L. Evans, "Convergence of an algorithm for mean curvature motion," in *Indiana Univ. Math. J.*, vol. 42, pp. 533-557, 1993.
- [6] G. Barles, C. Georgelin, "A simple proof of convergence of an approximation scheme for computing motions by mean curvature," in *SIAM J. Numer. Anal.*, vol. 32, pp. 484-500, 1995.
- [7] Y. Goto, K. Ishii, T. Ogawa, "Method of the distance function to the Bence-Merriman-Osher algorithm for motion by mean curvature," in *Comm. Pure Appl. Anal.*, vol. 4, pp. 311-339, 2005.
- [8] S. J. Ruuth, "A diffusion-generated approach to multiphase motion," in *J. Comp. Physics*, vol. 145, pp. 166-192, 1998.
- [9] R. Z. Mohammad, K. Svadlenka, "Multiphase Volume-preserving Interface Motions via Localized Signed Distance Vector Scheme", preprint.
- [10] R. Z. Mohammad, "Multiphase mean curvature flow: signed distance vector approach," in *Recent development in computational science: selected papers from the ISCS*, vol. 4, pp. 115-123, 2013.
- [11] L. Bronsard, F. Reitich, "On three-phase boundary motion and the singular limit of a vector-valued Ginzburg - Landau equation," in *Arch. Ration. Mech. Anal.*, vol. 124, pp. 355-379, 1993.
- [12] H. Garcke, B. Nestler, B. Stoth, "A multiphase field concept: numerical simulations of moving phase boundaries and multiple junctions," in *SIAM J. Appl. Math*, vol. 60, pp. 295-315, 1999.
- [13] H. Garcke, B. Nestler, B. Stoth, "On anisotropic order parameter models for multi-phase systems and their sharp interface limits," in *Physica D*, vol. 115, pp. 87-108, 1998.
- [14] X. Chen, J-S. Guo, "Self-similar solutions of a 2-D multiple-phase curvature flow," in *J. Comp. Physics*, D 229, pp. 22-34, 2007.
- [15] K. Ishii, "Mathematical analysis to an approximation scheme for mean curvature flow, in: S. Omata, K. Svadlenka (Eds.), ISCS 2011," in *Mathematical Sciences and Applications*, vol. 34, GAKUTO International Series, pp. 67-85, 2011.
- [16] E. Rothe, "Zweidimensionale parabolische Randwertaufgaben als Grenzfall eindimensionaler Randwertaufgaben," in *Math. Ann.*, vol. 102, pp. 650-670, 1930.
- [17] H. Zhao, T. Chan, B. Merriman, S. Osher, "A variational level set approach to multiphase motion", in *J. Comp. Physics*, vol. 127, pp. 179-195, 1996.
- [18] S. Osher, J. A. Sethian, "Fronts propagating with curvature dependent speed: Algorithms based on Hamilton-Jacobi formulations", in *J. Comp. Physics*, vol. 79, pp. 12-49, 1988.
- [19] D. Ševčovič and S. Yazaki, "On a gradient flow of plane curves minimizing the anisoperimetric ratio", in *IAENG International Journal of Applied Mathematics*, vol. 43 (3), pp. 160-171, 2013.

Nur Shofianah was born in Gresik, Indonesia, on November 24th, 1984. She received S.Si. degree and M.Si. degree in Mathematics from Sepuluh Nopember Institute of Technology, Surabaya, East Java, Indonesia, in 2007 and 2009, respectively.

In 2010, she joined the Departement of Mathematics, Faculty of Mathematics and Natural Sciences, University of Brawijaya, Indonesia, as a lecturer. Since October 2011, she takes Ph.D in Computational Science, Graduate School of Natural Science and Technology, Kanazawa University, Japan, by scholarship from Directorate General of Higher Education, Ministry of National Education, Indonesia. Her current research interests include interface dynamics and numerical solution of incompressible Navier-Stokes equations in moving domain using stabilized space-time finite element method.